Pupil shaping and coherence control in an EUV mask-imaging microscope

Iacopo Mochi*[a], Kenneth A. Goldberg, Markus P. Benk, Patrick P. Naulleau.
Lawrence Berkeley Laboratory, 1 Cyclotron Road, Berkeley, CA, USA 94720.

ABSTRACT

We are investigating the effect of pupil-fill patterns and partial coherence settings on EUV reticle images on the new SEMATECH High-NA Actinic Reticle review Project (SHARP), to deepen our understanding of its performance, and improve the emulation of image formation in arbitrary printing tools. SHARP is an EUV mask microscope developed as the successor of the SEMATECH Berkeley Actinic Inspection Tool (AIT). It is equipped with a unique, MEMS-based Fourier synthesis illuminator that generates arbitrary, customized pupil fill patterns to control the illumination partial coherence. The high-magnification objective lenses are an array of interchangeable Fresnel zoneplates with 4×NA values ranging from 0.25 to 0.625.

We have used SHARP to inspect isolated and dense features with half pitch as low as 55 nm using lenses with a range of NA values, and common illumination patterns, such as annular, dipole and QUASAR™. We will show the effect of illumination on important, measured pattern parameters, including contrast, normalized image log-slope, and depth of focus.

We have also studied the effect of partial coherence on the imaging of on multilayer roughness observed in bright mask regions, a topic important for expanding our understanding of the causes of LER.

Keywords: EUV lithography, EUV microscopy, mask inspection, coherence, pupil-fill.

1. INTRODUCTION

In EUV lithography, the partial coherence specifications of the light source play a fundamental role in the quality of the mask aerial image, as shown in Figure 1. We developed SHARP (The SEMATECH, High-NA Actinic Reticle review Project),[1] a synchrotron-based EUV microscope dedicated to mask imaging, featuring a Fourier synthesis illuminator[2] that can create a arbitrary partial coherence settings. SHARP was built on beamline 11.3.2 at the Advanced Light Source at Lawrence Berkeley National Laboratory. SHARP's illuminator can emulate the partial coherence of the printing tools the mask is intended for and provide greater understanding of the aerial image that will be printed. Moreover, SHARP can be used to investigate aerial image characteristics such as normalized intensity log slope (NILS), pattern edge roughness, contrast and depth of focus under various illumination patterns, performing a full characterization of the reticle with EUV light.

Figure 1. Three EUV images of LBNL logo collected with NA = 0.0625 and disk fill illumination with different partial coherence values. The diffraction effects induced by the pattern edges are clearly visible for low sigma while at high sigma a loss of contrast for high spatial frequencies can be observed.

SHARP allows us to quantify the effects of different pupil fills and partial coherence settings on EUV-reticle aerial images. Here we analyze the effects of different illumination settings on through-focus contrast, depth of focus, NILS and mask surface roughness. While SHARP features zoneplates with 4×NA values ranging from 0.25 to 0.625, for the

Photomask Technology 2013, edited by Thomas B. Faure, Paul W. Ackmann, Proc. of SPIE
Vol. 8880, 888022 · © 2013 SPIE · CCC code: 0277-786X/13/$18 · doi: 10.1117/12.2026498

experiments presented here, we used only one lens with 4×NA = 0.25 (NA = 0.0625), focal length f = 0.5 mm and a chief ray angle CRA = 6°.

1.1 SHARP Fourier Synthesis Illuminator

The synchrotron beam that powers SHARP is generated by a bending magnet; a monochromator selects the wavelength of operation with a bandwidth of 1/1500. The EUV beam is focused vertically by a single, elliptically bent mirror, and horizontally by a cylindrical mirror far upstream. At the beamline's intermediate focus, the beam divergence is 1.85×4.4 mrad, with an unconstrained beam spot size of ~200×300 μm.

SHARP's illuminator consists of three multilayer-coated mirrors called M_A, M_B and M_C, designed to reimage the beamline focus to the mask surface with a magnification of 0.1 and an angular distribution up to 20° off axis. The position of M_A coincides with the beamline's intermediate focus. M_A is a 1-mm diameter multilayer mirror mounted to a tip-tilt MEMS stage[3,4] created by Mirrorcle Technologies Inc. The reflected beam is reflected by M_B, a flat folding mirror up into the ellipsoidal condenser, M_C. The condenser mirror reimages the beam spot on M_A onto the mask surface.

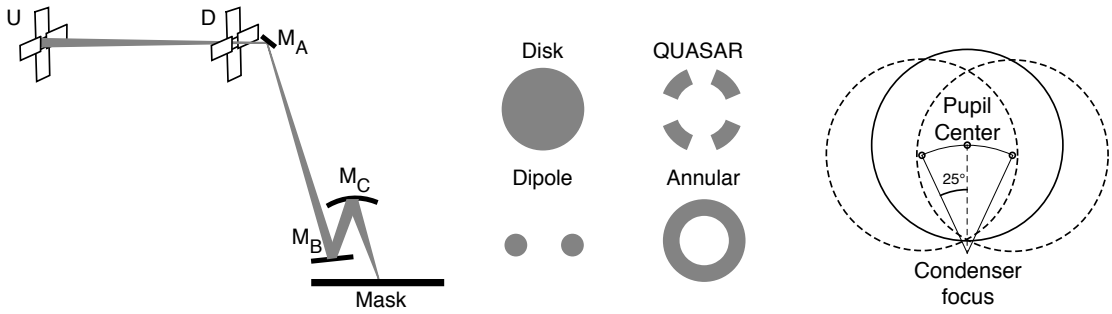

Figure 2. The Fourier synthesis illuminator of SHARP is designed to produce critical illumination for the microscope by reimaging the beamline intermediate focus, located on the surface of M_A, onto the sample reticle surface. By changing the angle of M_A we generate customized pupil fills. Some of the most used in lithography are disk fill, dipole, annular and QUASAR. The condenser mirror M_C is design to accommodate mask-side NA values up to 0.1525 in an azimuthal range of ± 25°.

The synchrotron beam is conditioned using two sets of xy slits. The downstream slits **D** are positioned close to M_A and control the beam size at focus. The upstream slits **U** are close to the output side of the vertical focusing mirror and allow us to limit the beam divergence, when necessary. The control of partial coherence is achieved by scanning the beam angle with M_A and "painting" the required pupil fill. The precision we can achieve in the definition of the pupil fill is limited by the divergence of the static beam. Neglecting the beam spot size, the static beam size on the microscope's imaging lens is given by:

$$\phi = \frac{p}{\cos\gamma}\sigma \,. \tag{1}$$

Where σ is the beam divergence, γ is the beam angle of incidence on the mask and p is the distance of the lens from the mask surface. The pupil fill is defined with an angular precision that is inversely proportional to the beam divergence, which means that, when needed, we can trade some flux for a better-defined pupil fill by closing the upstream slits.

We control the angular distribution of the beam by scanning the angle of M_A at high frequency during each exposure. The condenser of SHARP was designed to reach a maximum NA of 0.0156, and to emulate current scanners, we also included the ability to change the illumination azimuth in a range of ± 25° as shown in Figure 2. These specifications require the reflected beam **R** to cover an angular range of ± 0.9° around **x** and ± 1.3° around **y**. (See Figure 4) .

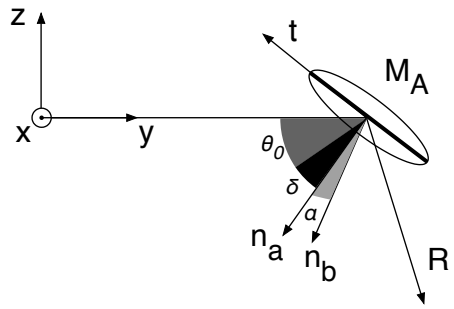

Figure 3. We control the tip-tilt of M_A around the **x** axis and the tangential vector **t**. The normal to the mirror's surface at rest forms an angle $\theta_0 = 55°$ with the direction of the incoming beam. When the mirror is tilted by α and δ, the reflected beam vector **R** tilts by $\tilde{\alpha}$ and $\tilde{\delta}$ as described by Eq. 2.

$$\tilde{\alpha} = \arctan\left(\frac{\cos(\delta+\theta_0)\sin(2\alpha)}{\cos^2(\alpha)\cos(2\delta)-\cos(2\theta_0)\sin^2(\alpha)}\right)$$
$$\tilde{\delta} = \arctan\left(\frac{\sin(2\delta)\cos(\alpha)^2+\sin(\delta)^2\sin(2\theta_0)}{\sqrt{\left(\cos^2(\alpha)\cos(2\delta)-\cos(2\theta_0)\sin^2(\alpha)\right)^2+\cos(\delta+\theta_0)^2\sin(2\alpha)^2}}\right) \quad (2)$$

We have control of the M_A tilt angle δ around **x** and α around **t**, therefore we use the coordinate transformation described by equation 2 that maps these two angles into $\tilde{\alpha}$ and $\tilde{\delta}$, the angles formed by the reflected vector **R** with its direction when M_A is in its rest position.

In practice, to achieve a better control over the M_A tip and tilt, we calibrate the angles empirically, using a pupil fill monitor (PFM). This device is a simple microscope built in the main chamber of SHARP that can visualize the illumination beam on a YAG crystal. The PFM can translate in 3D and can image the illumination beam in its focal plane and in the pupil plane. The angle calibration is performed by scanning the beam across the whole pupil area and creating a map of the beam angle as a function of the voltages used to drive M_A. This method allows us to check periodically the angle calibration and correct accidental misalignments that could result in systematic errors in the pupil fill.

1.2 Absorber reflectivity

Accurate measurements of line and pattern properties require knowledge of the finite reflectivity of the absorber. For the calculations presented in this paper, we quantify the absorber reflectivity relative to the reflectivity of the multilayer. To measure it, we compared the intensity of two series of images (1) collected over a clear region and (2) over an area covered with absorber. Each image was pre-processed by subtracting a camera background level that consists of dark current and a fixed offset. After background subtraction, we selected a 3×3 μm^2 portion of each image and calculated its best fitting plane to account for non-uniformities in the illumination. The average ratio between absorber intensity and the clear region intensity is an estimate of the absorber relative reflectivity. We repeated this procedure over 10 different areas of the mask and measured an average absorber reflectivity value, $R_{abs} = 0.012 \pm 0.0005$.

1.3 Lens flare

Flare is an undesirable property of the imaging lens can contribute a background intensity that reduces image contrast and affects the accurate measurement the line properties. To evaluate the lens flare in SHARP, we imaged a large dark, vertical line in a bright field at best focus, and measured the line intensity profile after background subtraction. (See Figure 2.) The lens resolution (with incoherent illumination) is $r = 1.22\ \lambda / 2\ NA = 131$ nm. For this test, we chose a line of 550 nm to limit the effect of the resolution on the line profile. We measured the intensity A of the light reflected by the multilayer and the intensity B in the center of the absorber line. We estimated the flare level F taking into account the reflectivity of the absorber using the relation $F = B / A - R = 1.0\%$.

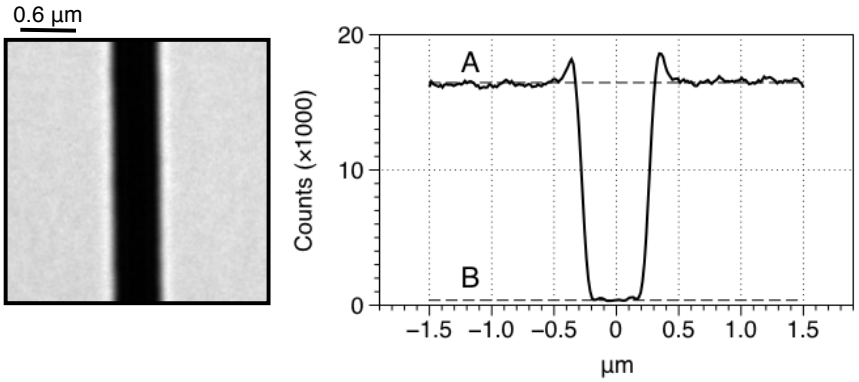

Figure 4. We estimated the lens flare for SHARP 0.0625 NA lens by collecting an image of a large (0.55 µm) dark line in a bright field.

2. PARTIAL COHERENCE AND CONTRAST

The illumination partial coherence has a direct effect on the resolution of a microscope[5,6]. We used SHARP to demonstrate the effect of partial coherence on the Contrast Transfer Function (CTF). We collected a series of through focus images of dense vertical lines of different sizes, varying σ from approximately 0 to 1. For each series we extracted the contrast from the best focus image, correcting for flare. Separately, we simulated the CTF for a mask with a relative absorber reflectivity $R_{abs} = 0.012$. As the partial coherence increases, the CTF curve rolls off more smoothly and the modulation of the lines extends toward smaller CD values; we also observe a drop in contrast for higher CD sizes.

The comparison of measurement and simulation shown in Figure 5 shows that, with the beam settings used in this experiment, the measured data agrees with the simulation for sigma as low as 0.6. For lower sigma values, the simulated curves that match the data have a higher partial coherence. In Figure 5 we show for example that if we program a pupil fill corresponding to a partial coherence of 0.1, we obtain a CTF that corresponds to a sigma value of 0.3. This mismatch is probably due to the fact that the minimum achievable partial coherence is dictated by the divergence of the synchrotron beam. We can increase the minimum partial coherence at the expenses of flux by reducing the size of the upstream aperture **U**. Another possible cause that we have identified may be a small ($\leq 0.5°$) error in the calibration of the M_A angle. With coherent light and line sizes close to the resolution of the imaging lens, small central ray angle errors could create problems of this nature.

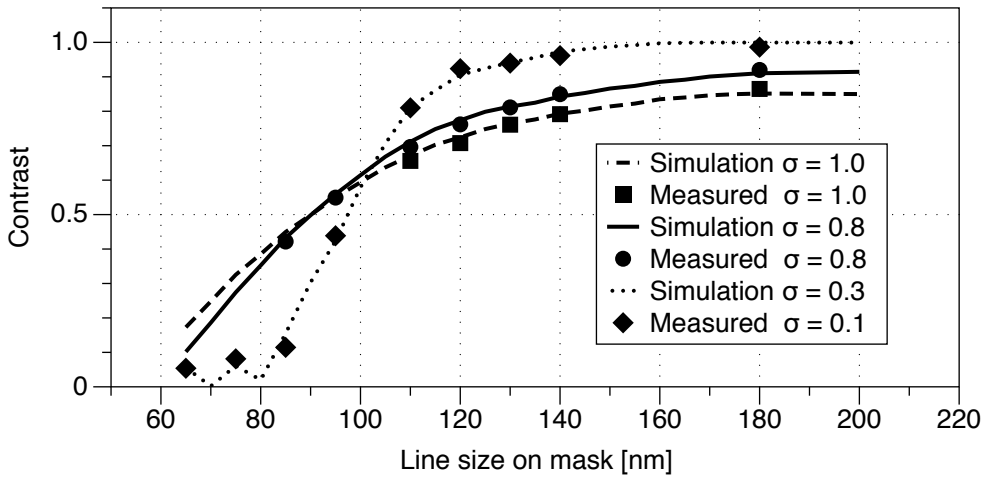

Figure 5. CTF curves at different partial coherence values for a SHARP zoneplate with NA = 0.0625 and disk-fill illumination.

3. DEPTH OF FOCUS

In lithography the concept of depth of focus (DOF) refers to the focus error range that produces acceptable results. The definition of acceptable results is somewhat arbitrary and depends on several metrics like line width and NILS. With SHARP we can create a visual representation of the depth of focus for a specific CD and numerical aperture as a function of partial coherence. Figure 6 shows a matrix of 1.5-μm-square EUV images through focus with different partial coherence settings. The lines are 110-nm half-pitch and the NA used is 0.0625 (0.25 4xNA) with disk fill illumination. This figure gives a quick idea of the DOF behavior as a function of σ. For low sigma values, contrast lobes appear through focus, due to the Talbot effect. The low contrast regions show the boundary to the DOF. At increased σ values, the overall contrast is lower, but the DOF expands.

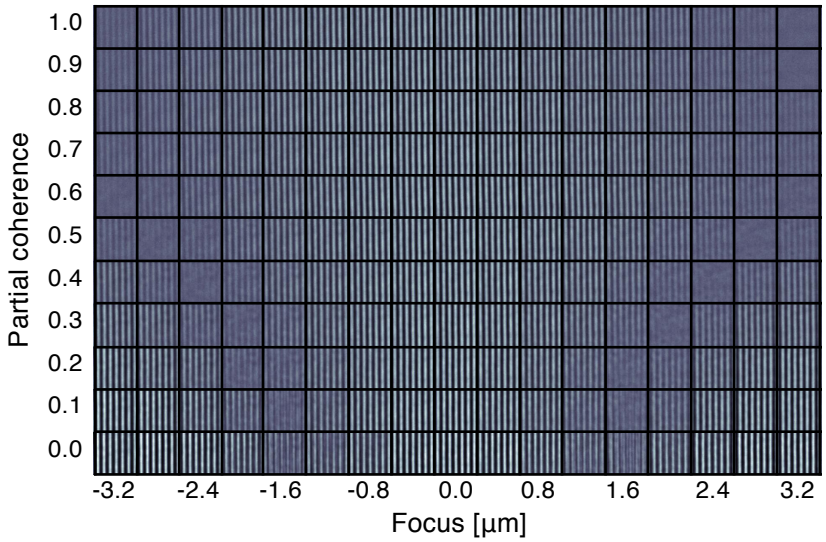

Figure 6. Through-focus EUV images of dense lines with different partial coherence at a fixed NA value. Each square has a size of 1.5 μm, the lines half pitch is 110 nm, and the numerical aperture is 0.0625. This compound image shows a visual representation of the DOF as a function of partial coherence.

For a quantitative evaluation of the DOF, we analyze the evolution of the aerial images through focus. This is done creating a focus-exposure matrix of the metric of interest[7].

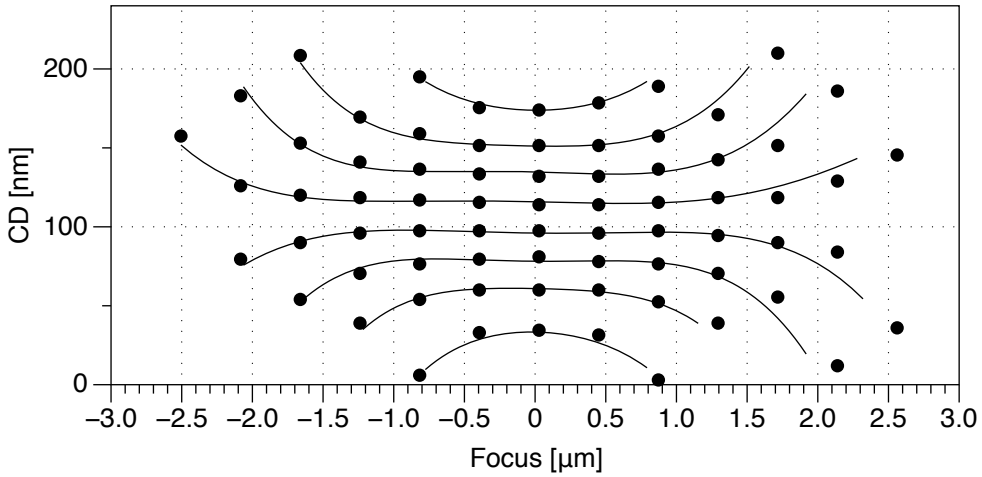

Figure 7. Bossung plot of a CD focus-exposure matrix of 110 nm vertical lines imaged with a 0.0625 NA lens. We used a disk-fill illumination with $\sigma = 0.5$. Each curve represents a different intensity level in the image from 6% to 94%. The original matrix was calculated using 100 levels. Here we show only 8 of them for clarity.

When analyzing the mask aerial images collected with SHARP, varying the intensity threshold simulates different exposure levels. The average dynamic range of the images collected with SHARP is 10,000–20,000 counts and can be increased up to about 60,000 counts with longer exposure times. This gives us a quasi-continuous image intensity profile. We measured the line width at 100 intensity levels spanning the intensity range and created a CD focus-exposure matrix. This matrix can be represented with a Bossung plot as shown in Figure 7 where each curve represents a different intensity level. The matrix gets fitted to a 2D polynomial of the form[7]:

$$CD = \sum_{i=0}^{3} \sum_{j=0}^{4} a_{ij} E^i F^j. \tag{3}$$

Where E is the exposure (in our case the intensity level) and F is the focus error. The curves shown in Figure 7 are obtained from the fit and the dots represent the measured data points. To calculate the DOF we set the acceptable range of CD values and of dose error. In this case we arbitrarily chose ±10% of the design CD value and ±5% of the intensity that yields the design CD. We draw the intensity curves relative to the chosen CD limits and we find the largest rectangle enclosed within the two curves with a height determined by the dose limits. The width of the rectangle is the DOF for the pattern under investigation. An example of this calculation is shown in Figure 8 where we used the CD FE matrix represented by the Bossung plot in Figure 7.

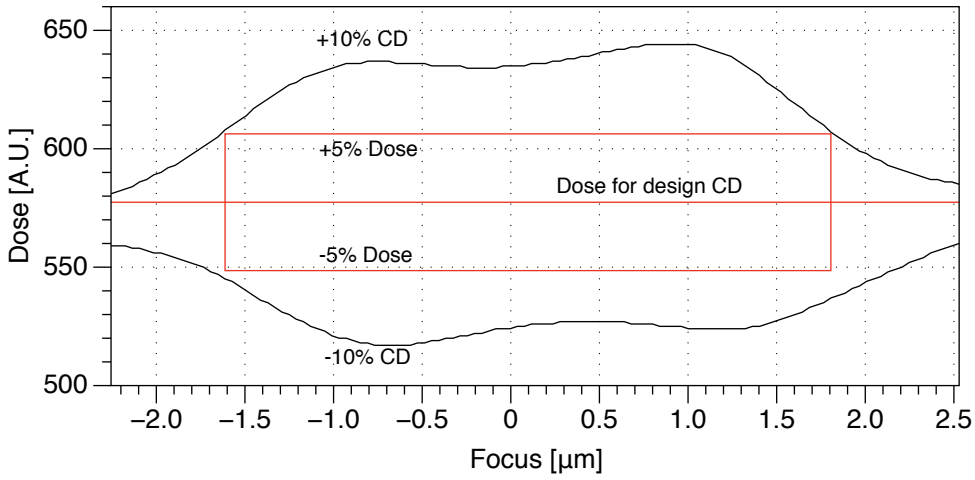

Figure 8. Depth of focus obtained from a CD focus-exposure matrix of 110 nm vertical lines imaged with a 0.0625 NA lens. We used a disk-fill illumination with $\sigma = 0.5$. We set the CD error as ± 10% of the design CD value and the dose error as ± 5% of the dose that produces the design CD value.

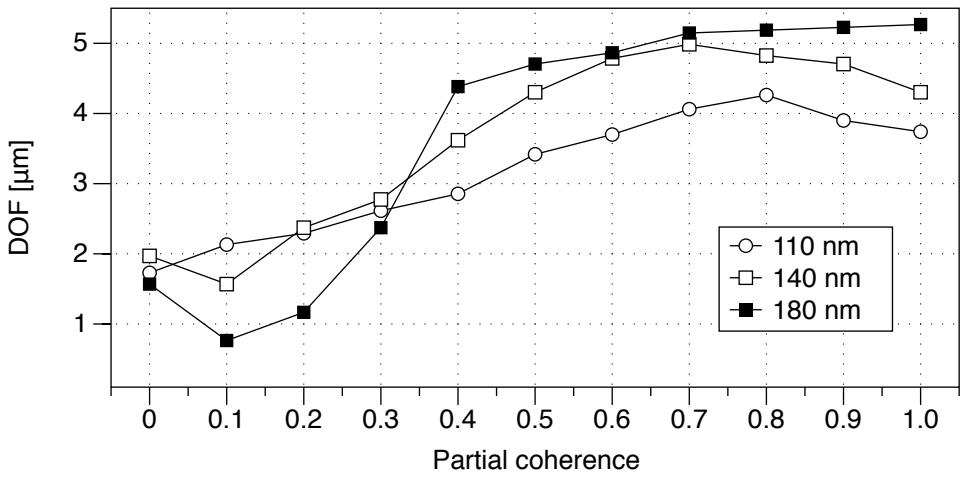

Figure 9. DOF calculated for three different lines sizes and different values of partial coherence. For the large lines at low σ values, the edge-diffraction effects reduce the DOF range. For smaller lines, the DOF reaches a peak at $\sigma \leq 1$, because of the contrast drop at high partial coherence predicted by the CTF curves.

We used this procedure to calculate the DOF of vertical lines of various sizes with different partial coherence values. For consistency we used a numerical aperture of 0.0624 (0.25 ×4 NA) and disk fill illumination. The results are presented in Figure 9 and show that the DOF increases with the partial coherence value, as already suggested by the composite image of Figure 6. It is also clear that the DOF reaches a peak for σ values between 0.7 and 0.8, at least for smaller line sizes (110 and 140 nm). This can be explained observing the CTF curves in Figure 5 that show how the contrast drops for high partial coherence values when the lines are larger than 100 nm.

4. NILS

Another metric widely used in lithography to assess image quality is NILS that is defined defined as:

$$\mathrm{NILS} = \mathrm{CD}\frac{1}{I}\frac{\partial I}{\partial x} \tag{4}$$

NILS provides information on the sharpness of the printed features and is therefore coupled with line width roughness[8]. We measured NILS as a function of half-pitch for three different sigma values. As the plot in Figure 10 shows, for dense lines wider than 100 nm, the highest NILS is achieved for lower σ values. In this way, high NILS occurs in conditions where the DOF is low and vice versa.

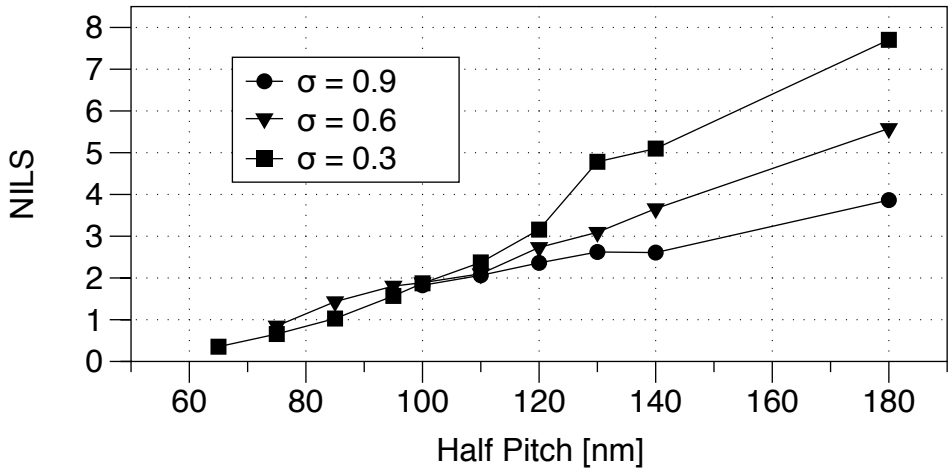

Figure 10. NILS measured as a function of dense line half-pitch for different σ values. Measurements were made with NA = 0.0625 (0.25 4×NA) and disk-fill illumination.

5. MASK SURFACE ROUGHNESS

Small perturbations in the multilayer structure, either propagated from the substrate or present in the multilayer itself, contribute to generate local phase variations in the beam reflected by the mask. Phase perturbations of the order of λ/30 are already sufficient to create significant effects in the aerial image[9] and can be generated by surface height variation of 0.25 nm or smaller. Surface roughness manifests itself as a speckle-like intensity pattern in the aerial image and, on a patterned mask, contributes to line edge roughness (LER). The source and the effects of mask surface roughness have become a greater concern as projection lithography CDs becomes smaller [8,10-14].

Mask surface roughness is inherently a phase effect and, as such, is strongly dependent on the partial coherence properties of the illumination. We used SHARP to visualize and quantify the effect of surface roughness on a blank mask by tiling through-focus images of 3.6-μm-square area, collected with different partial coherence values. Images were recorded with a 0.0625 NA (0.25 4xNA) and disk-fill illumination.

To quantify the effect of the roughness, we calculated the standard deviation of the normalized image intensity. The contour plot in Figure 11 shows how the intensity modulation from speckle is stronger for small σ values and how it increases as we move slightly out of focus.

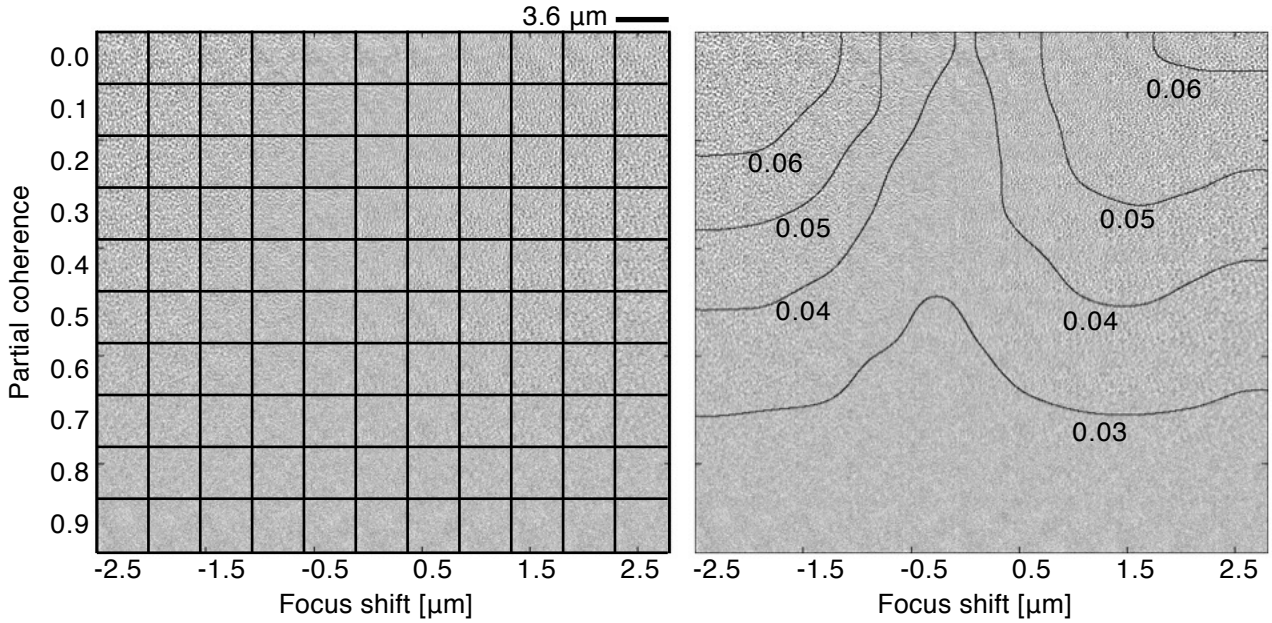

Figure 11. We visualize the mask roughness by tiling through-focus EUV images of a 3.6 µm-square of bare multilayer recorded using different partial coherence values. We used a lens with NA = 0.0625 (0.25 4×NA) and disk-fill illumination. On the right panel we superimposed the roughness contours to the same tiled image. The roughness is measured as the standard deviation of the normalized image intensity over each square.

6. CONCLUSIONS

Partial coherence and illumination control are among the key factors that determine the aerial image quality in lithographic projection systems. NILS, contrast, DOF, mask surface roughness are all strongly dependent on the coherence and on the pupil fill used to image the reticles. We demonstrated the ability of SHARP to shape the pupil fill and to control the illumination coherence in a flexible, lossless manner. The data provide examples of the effects that varying partial coherence has on the metrics commonly used to asses image quality in projection lithography. SHARP can be used to characterize the properties of reticles and to investigate, in detail, how illumination settings affect real-world EUV aerial images.

REFERENCES

[1] K. A. Goldberg, I. Mochi, M. Benk, A. P. Allezy, M. R. Dickinson, C. W. Cork, D. Zehm, J. B. Macdougall, E. Anderson, et al., "Commissioning an EUV mask microscope for lithography generations reaching 8 nm," Proc. SPIE 867919–10 (2013) [doi:10.1117/12.2011688].

[2] P. P. Naulleau, K. A. Goldberg, P. Batson, J. Bokor, P. Denham, and S. Rekawa, "Fourier-synthesis custom-coherence illuminator for extreme ultraviolet microfield lithography," *Applied Optics* **42**(5), 820–826, Optical Society of America (2003).

[3] Mirrorcle Technologies Inc., "Mirrorcle Technologies MEMS Mirrors–Technical Overview" (2009).

[4] V. Milanovic, "Multilevel Beam SOI-MEMS Fabrication and Applications," *J. Microelectromech. Syst.* **13**(1), 19–30 (2004) [doi:10.1109/JMEMS.2003.823226].

[5] R. S. Sirohi and G. S. Bhatnagar, "Effect of Partial Coherence on the Resolution of a Microscope," *Optica Acta: International Journal of Optics* **17**(11), 839–842 (1970) [doi:10.1080/713818258].

[6] M. Born and E. Wolf, *Principles of Optics: Electromagnetic Theory of Propagation, Interference and Diffraction of Light*, Cambridge University Press (1999).

[7] C. A. Mack, D. A. Legband, S. Jug, "Data Analysis for Photolithography" *Micro- and Nano-Engineering 98, Proc.*, and *MicroElectronic Engineering*, Vol. 46, Issues 1-4 (May 1999) pp. 65-68.
[8] C. A. Mack, "Impact of mask roughness on wafer line-edge roughness," Proc. SPIE 748828 (2009); doi:10.1117/12.834787.
[9] N. A. Beaudry and T. D. Milster, "Effects of object roughness on partially coherent image formation," *Optics letters* **25**(7), 454–456, (2000).
[10] S. A. George and P. P. Naulleau, "Extreme ultraviolet mask substrate surface roughness effects on lithographic patterning," *Journal of Vacuum Science & Technology B: Microelectronics and Nanometer Structures* **28**(6) (2010) [doi:10.1116/1.3502436].
[11] S. A. George, P. P. Naulleau, E. M. Gullikson, I. Mochi, F. Salmassi, K. A. Goldberg, and E. H. Anderson, "Replicated mask surface roughness effects on EUV lithographic patterning and line edge roughness," Proc. SPIE 79690E (2011).
[12] G. M. Gallatin and P. P. Naulleau, "Modeling the transfer of line edge roughness from an EUV mask to the wafer," Proc. SPIE 796903–10, (2011).
[13] B. M. McClinton and P. P. Naulleau, "Mask roughness induced LER control and mitigation: aberrations sensitivity study and alternate illumination scheme," Proc. SPIE 79691Z–1 (2011) [doi:10.1117/12.881678].
[14] B. M. McClinton and P. P. Naulleau, "Mask roughness induced LER: geometric model at long correlation lengths," Proc. SPIE 79691Y–8, International Society for Optics and Photonics (2011) [doi:10.1117/12.881677].